



# CHORUS

This is the accepted manuscript made available via CHORUS. The article has been published as:

## Viscous Rayleigh-Taylor instability in spherical geometry

Karnig O. Mikaelian

Phys. Rev. E **93**, 023104 — Published 8 February 2016

DOI: [10.1103/PhysRevE.93.023104](https://doi.org/10.1103/PhysRevE.93.023104)

# On the viscous Rayleigh-Taylor instability in spherical geometry

Karnig O. Mikaelian

*Lawrence Livermore National Laboratory, Livermore, California 94551, USA*

We consider viscous fluids in spherical geometry, a lighter fluid supporting a heavier one. Chandrasekhar (*Quart. J. Mech. Appl. Math.* **8**, 1 (1955)) analyzed this unstable configuration providing the equations needed to find, numerically, the exact growth rates for the ensuing Rayleigh-Taylor instability. He also derived an analytic, but approximate solution. We point out a weakness in his approximate dispersion relation (DR) and offer a somewhat improved one. A third DR, based on transforming a planar DR into a spherical one, suffers no unphysical predictions and compares reasonably well with the exact work of Chandrasekhar and a more recent numerical analysis of the problem (G. Terrones and M. D. Carrara, *Phys. Fluids* **27**, 054105 (2015)).

PACS numbers 47.20.Bp, 47.20.Gv, 47.20.Ma.

## I. INTRODUCTION

Hydrodynamic instabilities affect the flow of fluids in static or dynamic configurations. The Rayleigh-Taylor (RT) instability [1,2] affects fluids in a gravitational field  $g$  or when a fluid of density  $\rho_A$  accelerates another fluid of density  $\rho_B$  with  $\rho_A < \rho_B$ . An example is water ( $\rho_A = 1.0 \text{ g/cm}^3$ ) supporting honey ( $\rho_B = 1.4 \text{ g/cm}^3$ ).

Small, infinitesimal perturbations at their interface grow with time and cause the interpenetration of the two fluids. Lord Rayleigh [1] analyzed this “static” configuration and many subsequent studies, especially in spherical geometry, were concentrated on astrophysical applications [3]. We call this a “static” configuration because the average location of the interface, or the radius  $R$ , does not vary with time while interpenetration continues.

The “dynamic” configuration in which a fluid accelerates a heavier fluid was studied by G. I. Taylor [2]. “Dynamic” because in this case the average location of the interface or  $R$  does change as a result of a pressure gradient. The unstable configuration of a heavy fluid supported by a light fluid in a gravitational field pointing “down” becomes unstable when the same light fluid accelerates the heavy fluid “up”. This average, accelerating motion is also accompanied by fluid interpenetration. Taylor found that the same, exponentially growing instability found by Lord Rayleigh operates here also:  $\eta \sim \eta_0 e^{\gamma t}$  where  $\eta$ =amplitude of perturbations,  $t$ =time, and  $\gamma$  is the growth rate. In fact the same expression for  $\gamma$  (given below) applies to both the “static” and “dynamic” configuration if  $g$  is interpreted as a gravitational field in the former and as acceleration in the latter case. This is true in planar geometry only; in spherical or cylindrical geometry there are differences, discussed below.

Fluid properties and in particular viscosity affect the RT instability in either configuration, static or dynamic, and any geometry, planar or spherical/cylindrical. The higher the viscosity of either fluid, the slower the interpenetration, i.e. it reduces the growth rate. In this paper we study the effect of viscosity on the growth rate of the static configuration in spherical geometry. We propose a relatively simple analytic,

approximate formula for  $\gamma$  and compare it with previous work giving exact numerical results [3,4]. We also compare the proposed formula with another approximation given by Chandrasekhar [3].

Concerning the static and dynamic configurations, the reader should not be misled by the identity of the RT instability in these two configurations noted above; It happens only for the simplest, often called “classical” case: inviscid fluids in planar geometry. In spherical geometry, or when viscosity is present, the correspondence between the two configurations ceases. For the static case one looks for exponentially growing modes with the largest growth rate  $\gamma$ , usually called a “stability analysis.” For the dynamic case one must solve an “initial value problem” and, except for the classical case, does not evolve in a simple, exponential manner. These points will be discussed further in the next Section. We bring them up here just to note that the dynamic problem, first treated by Taylor [2], has acquired very substantial attention in recent years because of its importance in inertial confinement fusion [5,6]. State-of-the-art calculations are now performed with 3D (three dimensional) hydrocodes in spherical geometry including radiation, viscosity, *etc.* [7,8] all of which act to suppress, but not eliminate, the RT instability. Another instability, the Richtmyer-Meshkov (RM) instability [9,10] occurs when a shock passes through an interface. This is often treated as an instantaneous acceleration and is clearly of a dynamic nature and will not be examined here; the effect of viscosity on the RM instability was treated in [11].

In Sec. II we present and discuss the dispersion relation (DR) for the growth rate starting with the classical, planar inviscid case [1,2] and ending with the spherical viscous case [3,4]. In Sec. III we compare the approximate DRs with exact numerical results for

low  $A$  [3] and high  $A$  [4], where  $A$  is the Atwood number defined by  $A \equiv (\rho_B - \rho_A)/(\rho_B + \rho_A)$ . A third, simpler model is presented in Sec. IV and all 3 DRs are compared with the exact results of Chandrasekhar [3]. Conclusions are presented in Sec. V, and mathematical details are given in the appendix.

## II. DISPERSION RELATIONS

We start with the classical case [1,2]:

$$\gamma^2 - gkA = 0, \text{ planar inviscid,} \quad (1)$$

where  $k = 2\pi/\lambda$ ,  $\lambda$  being the wavelength of the perturbation in the shape of  $\eta(t)\cos(kx)$ . In this paper we discuss only the linear regime defined by  $\eta k \ll 1$ .

In the spherical case the shape is  $\eta(t)Y_{n,l}$  where  $Y_{n,l}$  is a spherical harmonic of order  $n$  and  $-n \leq l \leq n$ . Now the DR is given by

$$\gamma^2 - \frac{n(n+1)(\rho_B - \rho_A)g}{R[n\rho_B + (n+1)\rho_A]} = 0, \text{ spherical inviscid,} \quad (2)$$

where  $R$  is the radius of the interface. The linear regime translates into  $n\eta/R \ll 1$ . Eq. (2) reduces to Eq. (1) in the short wavelength limit,  $n \gg 1$ , as  $n/R \rightarrow k$ .

Eq. (2) has an interesting history. It was derived first by Binnie [12] and rederived by others [13,14]. Soon after Binnie's paper Plesset published a new analysis with a different result [15]. We have already commented [16] on the difference between Eq. (2) and Plesset's result. Some confusion has arisen from the fact that the authors [12-14] have claimed Eq. (2) as the solution for the dynamic problem where  $R = R(t)$  and  $g \equiv \ddot{R}$ , while Eq. (2) is the solution to the static problem with  $R = \text{const}$ . Plesset's solution, which we do not reproduce here, is the correct solution for the dynamical problem.

In contrast, the classical solution, Eq. (1), applies to both the static [1] and the dynamic [2] cases, the latter giving  $\eta(t) = \eta_0 \cosh(\gamma t)$  where  $\gamma = \sqrt{gkA}$ ,  $\eta_0 \equiv \eta(t=0)$ , and we have assumed  $\dot{\eta}_0 \equiv \left. \frac{d\eta}{dt} \right|_{t=0} = 0$ .

The above statements are not affected by the addition of surface tension  $T^{(s)}$  [17]: Static [1] and dynamic [2] treatments coincide for (and only for) the planar inviscid case. The “buoyancy” term  $gkA$  in Eq. (1) is multiplied by  $1 - k^2/k_c^2$  where  $k_c^2 \equiv (\rho_B - \rho_A)g/T^{(s)}$ . Note that this factor can be negative for  $k^2 > k_c^2$ , i.e. short wavelength perturbations, in which case the configuration becomes stable [17] and  $\cosh(\gamma t)$  converts to  $\cos(\gamma t)$  with  $\gamma = \{gkA(k^2/k_c^2 - 1)\}^{1/2}$ .

Matters are substantially complicated when we include viscosity [3,17]. In this paper we quote only approximate DRs and refer the reader to previous literature for the exact treatments. In planar geometry an approximate DR is

$$\gamma^2 + 2k^2\nu\gamma - gkA = 0, \text{ planar viscous,} \quad (3)$$

where  $\nu \equiv (\mu_B + \mu_A)/(\rho_B + \rho_A)$  and  $\mu_{A,B}$  are the viscosities of fluids A and B. The exact treatment can be found in Ref. 18 and was reviewed in [17].

Eq. (3) also has an interesting history. Bellman and Pennington [18] quote it as an upper bound on  $\gamma_{exact}$ . Shortly thereafter Hide derived it as an approximate DR [19] using a variational method due to Chandrasekhar [20] – see also Ref. [17]. Subsequently, Reid pointed out an error [21] in Hide’s derivation. Since then any reference to Hide’s work is accompanied by a reference to Reid’s work. Only the derivation of Eq. (3) was in question because comparisons have shown that the formula itself is an excellent approximation to the exact results [22,23].

In Ref. [11] we provided an alternative derivation of Eq. (3) which bypasses Reid's objection by applying a method used earlier to treat, again approximately, density gradient stabilization [24]. Here we use the same method, which is a simple variation on Chandrasekhar's technique, to derive an approximate DR (Eq. (6) below) for the spherical viscous case.

There is only one case, that of a planar, single, viscous fluid with a free surface, i.e.  $A=1$ , for which an exact growth rate is known analytically [25]. It is somewhat ironic that in comparing it with the approximate result, Eq. (3) above, we made an error by leaving out the factor of 2 that appears in Eq. (3). Upon converting to nondimensional variables  $X$  and  $Y$ , defined as  $k(\nu^2/g)^{1/3}$  and  $\gamma(\nu/g^2)^{1/3}$  respectively, Eq. (3) reads  $Y^2 + 2X^2Y - X = 0$  and therefore the solution is  $Y = -X^2 \pm \sqrt{X^4 + X}$  instead of Eq. (24) in Ref. 25. In effect, Fig. 2 in Ref. [25] compares the exact result for  $\nu$  (thick line) with the approximate result for  $\nu/2$  (thin line), which explains why the thin line is so much above the thick one. When compared for the *same* value of  $\nu$  the approximate solution is much *closer* to the exact one and practically coincides with it, unlike what is shown in Fig. 2 of Ref. [25].

Finally, we consider the spherical viscous problem and, again, write down only approximate viscous DRs. Using his variational principle Chandrasekhar derived

$$\gamma^2 + \frac{\{2n(n+1)[n\mu_B + (n+1)\mu_A] + (2n+1)^2(\mu_B - \mu_A)\}\gamma}{R^2[n\rho_B + (n+1)\rho_A]} - \frac{n(n+1)(\rho_B - \rho_A)g}{R[n\rho_B + (n+1)\rho_A]} = 0 \quad (4)$$

for the spherical viscous problem (Eq. (90) in Ref. [3]). He compared the above equation with his exact results for the case  $A=0.1$  and  $\nu_A = \nu_B$  and found good agreement – See Fig. 2 in [3]. Here  $\nu_A \equiv \mu_A/\rho_A$  and  $\nu_B \equiv \mu_B/\rho_B$ . Note that when  $\nu_A = \nu_B$  their common

value is given also by  $\nu$  as defined above,  $(\mu_A + \mu_B)/(\rho_A + \rho_B)$ . As expected, Eq. (4) reduces to Eq. (3) in the planar limit ( $n \rightarrow \infty, n/R \rightarrow k$ ) and to Eq. (2) in the inviscid limit ( $\mu_{A,B} \rightarrow 0$ ), and to the classical result, Eq. (1), in the planar inviscid limit.

Eq. (4), however, suffers in one aspect: It predicts a completely unphysical behavior, “negative viscosity,” for the lowest mode ( $n=1$ ) when  $\mu_A > 13\mu_B$ . For  $n=1$  Eq. (4) reduces to

$$\gamma^2 + \frac{(13\mu_B - \mu_A)\gamma}{R^2[\rho_B + 2\rho_A]} - \frac{2(\rho_B - \rho_A)g}{R[\rho_B + 2\rho_A]} = 0. \quad (5)$$

The “viscous term,” meaning the middle term in Eqs. (3)-(5), becomes negative in Eq. (5) if  $\mu_A > 13\mu_B$ , implying growth faster (!) than inviscid. One can show that this is the only anomaly of Eq. (4): For  $n \geq 2$  the viscous term is always positive as long as  $\mu_{A,B} > 0$ , hence the usual behavior is obtained: viscous growth is slower than inviscid growth.

The above observation led us to consider our simpler method to derive approximate DRs [24]. For the density gradient application we obtained a different DR [24]. For the planar viscous problem we obtained the same DR [11]. For the spherical viscous problem at hand we obtain

$$\gamma^2 + \frac{2n(n+1)[(n+2)\mu_B + (n-1)\mu_A]\gamma}{R^2[n\rho_B + (n+1)\rho_A]} - \frac{n(n+1)(\rho_B - \rho_A)g}{R[n\rho_B + (n+1)\rho_A]} = 0, \quad (6)$$

which is derived in the appendix. We believe this is an improvement over Eq. (4).

However, it still has an unphysical prediction for  $n=1$ :

$$\gamma^2 + \frac{12\mu_B\gamma}{R^2[\rho_B + 2\rho_A]} - \frac{2(\rho_B - \rho_A)g}{R[\rho_B + 2\rho_A]} = 0. \quad (7)$$

Although it does not predict “negative viscosity” like Eq. (5), Eq. (7) predicts that if  $\mu_B = 0$  then the growth is inviscid, independently of  $\mu_A$ . We expect, on simple physical grounds, that growth should be suppressed even if only one of the fluids (the lighter one in this case) has viscosity.

In Eq. (6) it is again clear that  $n = 1$  is the only possible anomalous case and that all modes  $n \geq 2$  are affected by viscosity as long as it is present in at least one of the fluids. Of the two anomalies displayed in Eq. (5) and (7) we believe the second one is less severe, so perhaps Eq. (6) is “less wrong” than Eq. (4). A simpler, somewhat *ad hoc* but anomaly-free DR will be discussed in Sec. IV.

The reader may inquire why Chandrasekhar, who did consider  $n = 1$ , did not point out this anomaly. The reason, most probably, was that in computing exact growth rates and then comparing them with his approximate DR (Eq. (4) above) he set  $\nu_A = \nu_B$ .

Setting  $\nu_A = \nu_B = \nu$  in Eqs. (4) and (6) we obtain

$$\gamma^2 + \frac{\nu}{R^2} \left\{ 2n(n+1) + \frac{(\rho_B - \rho_A)(2n+1)^2}{n\rho_B + (n+1)\rho_A} \right\} \gamma - \frac{n(n+1)(\rho_B - \rho_A)g}{R[n\rho_B + (n+1)\rho_A]} = 0 \quad (8)$$

and

$$\gamma^2 + \frac{2n(n+1)\nu}{R^2} \left\{ 1 + \frac{2(\rho_B - \rho_A)}{n\rho_B + (n+1)\rho_A} \right\} \gamma - \frac{n(n+1)(\rho_B - \rho_A)g}{R[n\rho_B + (n+1)\rho_A]} = 0 \quad (9)$$

respectively. Eq. (8) above appears as Eq. (91) in [3]. Since  $\rho_B > \rho_A$  neither of the above two equations displays any anomaly. Even for  $n = 1$  the viscous term is

$$(\nu/R^2) \left[ 4 + \frac{9(\rho_B - \rho_A)}{\rho_B + 2\rho_A} \right] \gamma \text{ in Eq. (8), compared with } (\nu/R^2) \left[ 4 + \frac{8(\rho_B - \rho_A)}{\rho_B + 2\rho_A} \right] \gamma \text{ from Eq.}$$

(9), quite similar.

In the next section we compare Eqs. (4) and (6) with each other and with the exact results of [3] for low  $A$ ,  $A = 0.1$ , and with the exact results of [4] for high  $A$ ,  $A = 1.0$ .

### III. COMPARISON

#### A. LOW $A$

Chandrasekhar [3] and Terrones and Carrara [4] chose different ways to reduce the number of variables and deal with nondimensional quantities. It is straightforward to show that the 8 primitive variables of the problem  $\gamma$ ,  $\rho_A$ ,  $\rho_B$ ,  $\mu_A$ ,  $\mu_B$ ,  $R$ ,  $g$ , and  $n$  can be combined into 5 nondimensional quantities. Chandrasekhar chose  $A$ ,  $\nu_A/\nu_B$ ,  $gR^3/\nu^2$ , and  $n$  as the 4 independent variables and  $\gamma\sqrt{R/g}$  as the dependent one, so  $\gamma\sqrt{R/g} = f(A, \nu_A/\nu_B, gR^3/\nu^2, n)$ . In his numerical work he took  $A = 0.1$ ,  $\nu_A/\nu_B = 1$ , and computed  $\gamma\sqrt{R/g}$  as a function of  $n$ ,  $n = 1-9$ , for 18 different values of  $gR^3/\nu^2 \equiv G$ , a ‘‘Grashoff’’ number.

In Fig. 1 we plot Eqs. (8) and (9) to be compared with Fig. 1 of [3]. As anticipated, both equations yield very similar results because of the choice  $\nu_A = \nu_B$ . It follows that the comparison with exact results made in Fig. 2 of [3] applies, practically with no change at all, to Eq. (8) as well as to Eq. (9).

#### B. High $A$

A different choice of variables was made by Terrones and Carrara [4]. They define

$$\alpha \equiv \gamma(\nu_B/g^2)^{1/3} \quad (10)$$

as a nondimensional growth rate, and take  $s \equiv \mu_A / \mu_B$ ,  $d \equiv \rho_A / \rho_B$ ,  $B \equiv R(g/v_B^2)^{1/3}$ , and again  $n$  as the 4 independent variables, i.e.,  $\alpha = \alpha(s, d, B, n)$ . They look at the case  $s = 0$ ,  $d = 0$  (hence  $A = 1$ ) and study  $\alpha$  as a function of  $n$  for various values of  $B$  – See Fig. 5 of [4].

For  $\mu_A = \rho_A = 0$  Eqs. (8) and (9) reduce to

$$\alpha^2 + [2(n+1)(n+2) + 1/n]\alpha / B^2 - (n+1)/B = 0 \quad (11)$$

and

$$\alpha^2 + 2(n+1)(n+2)\alpha / B^2 - (n+1)/B = 0 \quad (12)$$

respectively. They differ only by  $1/n$  in the viscous term which obviously is negligible for large  $n$  (as stated above for any  $\mu_{A,B}$  and  $\rho_{A,B}$  both DRs given in Eqs. (4) and (6) go over to the planar limit, Eq. (3), for large  $n$ ). For  $n = 1$  the coefficient of the viscous term is 13 in Eq. (11) and 12 in Eq. (12) so we again expect small differences between the two, mostly at low  $B$ , i.e. high viscosity. Note that  $G$  and  $B$  are related by  $G = B^3$ .

In Fig. 2 we plot  $\alpha$  from Eqs. (11) and (12) as functions of  $n$ ,  $n = 1 - 50$ , for  $B = 1, 2, 5, 10$ , and  $50$ , to be compared with Fig. 5a of Terrones and Carrara [4]. Clearly, the two approximate DRs yield very similar growth rates and, compared with the exact results of [4], the agreement is quite good except for low values of  $n$  and  $B$ . This is confirmed by Fig. 3 where we again plot  $\alpha$  from Eqs. (11) and (12) for  $n = 1 - 7$  and  $B = 0.1, 1, 2$ , and  $5$ . This figure should be compared with Fig. 5b of [4].

To highlight the differences let us look at the point  $n = B = 1$ . From Eq. (11),  $\alpha^2 + 13\alpha - 2 = 0$ , we get  $\alpha = (-13 + \sqrt{177})/2 \approx 0.152$ , and from Eq. (12) we get  $\alpha = -6 + \sqrt{38} \approx 0.164$ . Both of these numbers are lower than the value, about 0.25, from

[4]. But for  $n = 7$  both equations give  $\alpha \approx 0.056$  in closer agreement with Ref. [4] giving  $\alpha \approx 0.067$  – See their Fig. 5b.

The advantages of having an explicit DR are obvious: One can calculate the growth rate for any given values of the 7 independent variables listed above. Exact results must be calculated numerically [3,4]. Another quantity, called  $B_{threshold}$  by Terrones and Carrara and related to  $G_{critical}$  of Chandrasekhar is defined as that value of  $B$  for which  $\gamma_{max}(n) = \gamma_{max}(n+1)$ . We propose calculating  $B_{threshold}(n)$  by treating  $n$  as a continuous variable and finding  $\gamma_{max}$  by setting  $\partial\gamma/\partial n = 0$ . A somewhat lengthy but straightforward calculation from Eq. (11), setting  $\partial\alpha/\partial n = 0$ , gives

$$B_{threshold}^3 = 4[2n + 3 - 1/2n^2][(n+1)^2 - 1/n - 1/2n^2]. \quad (13)$$

A simpler calculation from Eq. (12) yields

$$B_{threshold}^3 = 4(2n + 3)(n+1)^2. \quad (14)$$

Note that both equations give  $B_{threshold} \rightarrow 2n$  in the large- $n$  limit. In Table I we compare  $B_{threshold}$  calculated from Eqs. (13) and (14) with the exact values given in Ref. [4].

#### IV. SIMPLE MODEL

In this section we consider a simple DR for the spherical viscous case. Eqs. (4) and (6) were based on approximations to the exact work of Chandrasekhar. An alternative, admittedly simple-minded approach, is the following: For the inviscid cases given by Eqs. (1) and (2), to go from planar (Eq. (1)) to spherical (Eq. (2)) geometry, one can define

$$k_n \equiv \frac{2n(n+1)}{R(2n+1-A)} \quad (15)$$

and replace  $k \rightarrow k_n$  in Eq. (1) to arrive at Eq. (2). We do the same for the viscous case:

Replace  $k \rightarrow k_n$  in Eq. (3) to arrive at

$$\gamma^2 + 2k_n^2 \nu \gamma - g k_n A = 0, \text{ spherical viscous.} \quad (16)$$

Like the two previous DRs, this one also reproduces the inviscid DR, Eq. (2), and the viscous planar DR, Eq. (3), in the appropriate limits of  $\nu \rightarrow 0$  and  $k_n \rightarrow k$  respectively.

The main advantage, needless to say, is that Eq. (16) has no “negative” or “zero” viscosity which were the weak points of Eqs. (4) and (6). In long form Eq. (16) reads

$$\gamma^2 + \frac{4n^2(n+1)^2(\mu_B + \mu_A)\gamma}{R^2(2n+1-A)[n\rho_B + (n+1)\rho_A]} - \frac{n(n+1)(\rho_B - \rho_A)g}{R[n\rho_B + (n+1)\rho_A]} = 0. \quad (17)$$

In Fig. 4 we compare Eqs. (4), (6), and (17) with Chandrasekhar’s exact results. This figure should be compared with Fig. 2 in [3]. All 3 DRs straddle the exact results.

Similarly, no noticeable difference is seen when we turn to the  $A=1$  problem considered by Terrones and Carrara [4] – All 3 DRs give similar results. Setting  $\mu_A = \rho_A = 0$  in Eq. (17) we obtain

$$\alpha^2 + 2(n+1)^2 \alpha / B^2 - (n+1) / B = 0 \quad (18)$$

with  $\alpha$  and  $B$  as defined earlier. Compare the above equation with Eqs. (11) and (12).

As discussed in subsection IIIB, for  $n = B = 1$  Eqs. (11) and (12) give  $\alpha \approx 0.152$  and  $0.164$  respectively. Eq. (18) above reduces to  $\alpha^2 + 8\alpha - 2 = 0$  and hence  $\alpha = -4 + \sqrt{18} \approx 0.243$ , much closer to the exact result  $0.25$  [4]. For  $n = 7$  Eqs. (11) and (12) gave  $\alpha \approx 0.056$ , while Eq. (18) above gives  $\alpha \approx 0.062$ , in somewhat better agreement with the exact result ( $\approx 0.067$ ) of Ref. [4].

Finally, we consider  $B_{threshold}$ . Calculating  $\alpha$  from Eq. (18) by setting  $\partial\alpha/\partial n = 0$  we get

$$B_{threshold} = 2(n + 1), \quad (19)$$

to be compared with Eqs. (13) and (14). For  $n = 1 - 4$  Eq. (19) predicts  $B_{threshold} = 4, 6, 8,$  and 10, in somewhat poorer, but perhaps still acceptable agreement with the numbers in Table I. Like Eqs. (13) and (14) it predicts  $B_{threshold} \rightarrow 2n$  in the large- $n$  limit.

## V. CONCLUSIONS

We have examined three, successively simpler DRs for the spherical viscous problem: Eq. (4) derived in [3]; Eq. (6) derived in our Appendix; and Eq. (17) more in the form of an *ansatz*.

Eq. (4) suffers from predicting “negative viscosity” for the case  $n = 1$  and  $\mu_A > 13\mu_B$ . Eq. (6) suffers from predicting “zero viscosity” for the case  $n = 1$  and  $\mu_B = 0$ , even when  $\mu_A > 0$ . Eq. (17) suffers no such unphysical behavior, predicting that viscous effects will vanish if and only if both  $\mu_A = 0$  and  $\mu_B = 0$ , just as in planar geometry. Given its simplicity and its acceptable comparison with the exact results of [3] and [4], we believe this simple *ansatz* can be used as an estimate for viscous effects in spherical geometry.

As Figs. 2-4 show, the main difference among the models occurs for  $n = 1$  and higher values of  $n$  do not discern among the models. Although most of the numerical simulations for NIF capsules [7,8] have focused on  $n \approx 2 - 100$ , there have been a few experiments searching exclusively for  $n = 1$  effects [26].

We have differentiated between the “static”,  $R = \text{const.}$ , and the “dynamic,”  $R = R(t)$  problems. The above DRs solve only the static problem. The dynamic problems are much more challenging and, in increasing complexity, are: inviscid spherical [15], viscous planar [27], and viscous spherical [28], the last one requiring the solution of an integro-differential equation. Exact solutions to viscous dynamic problems are practically out of the question, and we hope the approximate growth rates presented in this work will be useful in future searches for approximate solutions.

#### ACKNOWLEDGMENT

I am grateful to Professors R. Rosensweig and T. Theofanous who independently pointed out my error in omitting a factor of 2 in Ref. [25]. This work was performed under the auspices of the U. S. Department of Energy by Lawrence Livermore National Laboratory under Contract DE-AC52-07NA27344.

#### APPENDIX: DERIVATION OF EQ. (6)

Start with Eq. (70) of Ref. [3]:

$$\begin{aligned}
 & -\gamma \frac{d}{dr} \left\{ \rho \frac{d}{dr} (rW) \right\} + n(n+1) \gamma \rho \frac{W}{r} - \frac{n(n+1)}{\gamma} \frac{g}{r} \frac{d\rho}{dr} W + \frac{d^2}{dr^2} (\mu r F) \\
 & - 2 \frac{d}{dr} \left\{ \frac{1}{r} \frac{d\mu}{dr} \frac{d}{dr} (rW) \right\} + 2n(n+1) \frac{1}{r} \frac{d^2 \mu}{dr^2} W - n(n+1) \frac{\mu}{r} F = 0
 \end{aligned} \tag{A1}$$

where

$$F \equiv \left\{ \frac{d^2}{dr^2} + \frac{2}{r} \frac{d}{dr} - \frac{n(n+1)}{r^2} \right\} W, \quad (\text{A2})$$

and  $W$  is the perturbed velocity. As in the planar case [11] we integrate the above equation from 0 to  $\infty$  and, as an approximation, use the inviscid eigenfunctions for  $W$  :

$$\begin{aligned} W_{\text{inviscid}} &= r^n, & r \leq 1 \\ &= r^{-(n+1)}, & r \geq 1, \end{aligned} \quad (\text{A3})$$

after normalizing  $r$  by the radius  $R$  of the interface, so that  $r=1$  denotes the interface (see Eq. (87) in [3]). Eq. (A1) has yet to be normalized in the same way. After integration by parts all “surface terms,” evaluated at  $r=0$  and  $r=\infty$ , are set to zero.

The 1<sup>st</sup>, 4<sup>th</sup>, and 5<sup>th</sup> terms in Eq. (A1) are total derivatives and therefore turn into surface terms upon integration and do not contribute. The last term also does not contribute because  $F=0$  in the approximation  $W \rightarrow W_{\text{inviscid}}$  (substitute Eq. (A3) in Eq. (A2)). Only the 2<sup>nd</sup>, 3<sup>rd</sup>, and 6<sup>th</sup> terms in Eq. (A1) will survive and, as will see, contribute to the first, last, and middle terms, respectively, of Eq. (6).

After performing the normalization the integrals in Eq. (A1) are:

$$\int_0^\infty \rho \frac{W}{r} dr = \rho_A \int_0^1 \frac{W}{r} dr + \rho_B \int_1^\infty \frac{W}{r} dr = \rho_A \int_0^1 r^{n-1} dr + \rho_B \int_1^\infty r^{-n-2} dr = \frac{\rho_A}{n} + \frac{\rho_B}{n+1}. \quad (\text{A4})$$

$$\int_0^\infty \frac{d\rho}{dr} \frac{W}{r} dr = \int_0^\infty (\rho_B - \rho_A) \delta(r-1) \frac{W}{r} dr = \rho_B - \rho_A. \quad (\text{A5})$$

$$\begin{aligned} \int_0^\infty \frac{d^2 \mu}{dr^2} \frac{W}{r} dr &= \int_0^\infty \mu \frac{d^2}{dr^2} \left( \frac{W}{r} \right) dr = \mu_A \int_0^1 \frac{d^2}{dr^2} \left( \frac{W}{r} \right) dr + \mu_B \int_1^\infty \frac{d^2}{dr^2} \left( \frac{W}{r} \right) dr \\ &= \mu_A \frac{d}{dr} \left( \frac{W}{r} \right) \Big|_{r=1_-} - \mu_B \frac{d}{dr} \left( \frac{W}{r} \right) \Big|_{r=1_+} = \mu_A (n-1) + \mu_B (n+2). \end{aligned} \quad (\text{A6})$$

We have used integration by parts twice in the first line of Eq. (A6).

As mentioned above only the 2<sup>nd</sup>, 3<sup>rd</sup>, and 6<sup>th</sup> terms in Eq. (A1) contribute to the integration. All of them have the common factor  $n(n+1)$  which can be canceled. Substituting Eqs. (A4), (A5), and (A6), respectively, in those three terms and including the  $R$  factors for normalization we obtain

$$\gamma \left( \frac{\rho_A}{n} + \frac{\rho_B}{n+1} \right) - \frac{(\rho_B - \rho_A)g}{\gamma R} + 2[\mu_A(n-1) + \mu_B(n+2)]/R^2 = 0 \quad (\text{A7})$$

which leads to Eq. (6).

Clearly, one can multiply Eq. (A1) by any power of  $W$ , say  $W^m$ , and then integrate. We advocated  $m=0$ , i.e. no multiplication at all [24]. Chandrasekhar's method corresponds to  $m=1$ . It is equally clear that if one could use the exact eigenfunction  $W_{exact}$ , then the calculated growth rate would be  $\gamma_{exact}$  and independent of  $m$ . However, not only  $W_{exact}$  is quite complicated, but to obtain it one already needs  $\gamma_{exact}$  and hence the process (multiplying by  $W_{exact}^m$  and integrating over space) would be a mere mathematical exercise. By using  $W_{approximate} = W_{inviscid}$ , which are much simpler and already at hand, one derives an approximate  $\gamma$  which depends on  $m$ , as illustrated by the two DRs in Eq. (4) and Eq. (6). The reader can readily appreciate the simplicity of our method (no multiplication) because, if one does multiply Eq. (A1) by  $W$  before integrating, as Chandrasekhar did, then the total derivative terms, viz. the 1<sup>st</sup>, 4<sup>th</sup>, and 5<sup>th</sup> terms in Eq. (A1) which did not contribute for us, must be kept and, after repeated integration by parts, evaluated using  $W_{approximate}$  in the final step, leading to Eq. (90) in Ref. [3].

The main reason why the DR based on  $m = 1$  differs from the DR based on  $m = 0$  is that  $W_{approximate}$  does not satisfy the requirement that not only  $W$  but  $dW/dr$  also must be continuous at the interface. Eq. (A3), the inviscid eigenfunction used as approximation to  $W$ , is continuous but its derivative is not. Chandrasekhar's solution was to take the average of the two terms containing  $dW/dr$  which he characterized as "admittedly a crude procedure," – see his discussion following Eqs. (88) and (89) in Ref. [3]. By not introducing an extra factor of  $W$  and integrating Eq. (A1) directly we bypass this issue and obtain a DR, Eq. (6), that is "less wrong" than Chandrasekhar's, given here as Eq. (4).

As to the replacement  $k \rightarrow k_n$ , one can justify it only for large- $n$  because spherical harmonics approach sinusoidal perturbations of wavelength  $\lambda = 2\pi/k \rightarrow 2\pi/k_n \approx 2\pi R/n$ . For arbitrary  $n$  we can only call upon the analogy with the inviscid case. The resulting DR, Eq. (17), avoids the anomalies suffered by the other two spherical DRs, Eqs. (4) and (6), and appears to be in reasonable agreement with the exact results of Chandrasekhar [3] and of Terrones and Carrara [4]. It remains to be seen whether such an extremely simple treatment is viable in other applications.

## **References**

- [1] Lord Rayleigh, *Scientific Papers*, **2**, ( Dover, New York, 1965).
- [2] G. I. Taylor, Proc. R. Soc. London Ser. A **201**, 192 (1950).
- [3] S. Chandrasekhar, Quart. J. Mech. Appl. Math. **8**, 1 (1955).
- [4] G. Terrones and M. D. Carrara, Phys. Fluids **27**, 054105 (2015).

- [5] J. Nuckolls, L. Wood, A. Thiessen and G. Zimmerman, *Nature* **239**, 139 (1972).
- [6] J. D. Lindl, *Inertial Confinement Fusion* (Springer, New York, 1998).
- [7] C. R. Weber *et al.*, *Phys. Rev. E* **89**, 053106 (2014).
- [8] D. S. Clark *et al.*, *Phys. Plasmas* **22**, 022703 (2015).
- [9] R. D. Richtmyer, *Commun. Pure Appl. Math.* **13**, 297 (1960).
- [10] E. E. Meshkov, *Fluid Dyn.* **4**, 101 (1969).
- [11] K. O. Mikaelian, *Phys. Rev. E* **47**, 375 (1993).
- [12] A. M. Binnie, *Proc. Cambridge Philos. Soc.* **49**, 151 (1953).
- [13] N. K. Gupta and S. V. Lawande, *Phys. Rev. A* **33**, 2813 (1986).
- [14] R. Epstein, *Phys. Plasmas* **11**, 5114 (2004).
- [15] M. S. Plesset, *J. Appl. Phys.* **25**, 96 (1954).
- [16] K. O. Mikaelian, *Phys. Rev. A* **36**, 411 (1987).
- [17] S. Chandrasekhar, *Hydrodynamic and Hydromagnetic Stability* (Oxford University Press, London, 1968).
- [18] R. Bellman and R. H. Pennington, *Q. Appl. Math.* **12**, 151 (1954).
- [19] R. Hide, *Proc. Cambridge Philos. Soc.* **51**, 179 (1955).
- [20] S. Chandrasekhar, *Proc. Cambridge Philos. Soc.* **51**, 162 (1955).
- [21] W. H. Reid, *Proc. Cambridge Philos. Soc.* **57**, 415 (1961).
- [22] A. J. Willson, *Proc. Cambridge Philos. Soc.* **61**, 595 (1965).

- [23] R. Menikoff, R. C. Mjolsness, D. H. Sharp , and C. Zemach, Phys. Fluids **20**, 2000 (1977).
- [24] K. O. Mikaelian, Phys. Rev. A **33**, 1216 (1986).
- [25] K. O. Mikaelian, Phys. Rev. E **54**, 3676 (1996).
- [26] B. K. Spears, M. J. Edwards, S. Hatchett, J. Kilkenny, J. Knauer, J. Lindl, D. Munro, P. Patel, H. F. Robey, and R. P. J. Town, Phys. Plasmas **21**, 042702 (2014).
- [27] A. Prosperetti, Phys. Fluids **24**, 1217 (1981).
- [28] A. Prosperetti, Quart. App. Math. **34**, 339 (1977).

### **Figure Captions**

Fig. 1. (Color online) Plot of the nondimensional growth rate  $\gamma\sqrt{R/g}$  as a function of mode number  $n$  for 11 values of the Grashoff number indicated on each pair of curves. The Atwood number is 0.1 and the viscosities satisfy  $\nu_A = \nu_B = \nu$ . Eq. (8), which is Eq. (91) in [3], is plotted as a dotted red line, and Eq. (9) is plotted as a solid black line. The two are practically indistinguishable. Compare with Fig. 1 in Ref. [3].

Fig. 2. (Color online) Nondimensional growth rate  $\alpha$  as a function of mode number  $n$  for 5 values of  $B$  as indicated on each pair of curves, for the case  $\mu_A = \rho_A = 0$ . Eq. (11) is plotted as dotted red line, and Eq. (12) is plotted as solid black line; the two are barely distinguishable. Compare with Fig. 5a of Ref. [4].

Fig. 3. (Color online) Same as Fig. 2 for 4 different values of  $B$ . Eqs. (11) and (12) can be distinguished at low values of mode number  $n$ . Compare with Fig. 5b of Ref. [4].

Fig. 4 (Color online) Comparison of the 3 approximate DRs with the exact results of Chandrasekhar [3] for the case  $A=0.1$  and  $\nu_A = \nu_B = \nu$ . All 3 DRs give similar results. We plot  $\gamma\sqrt{R/g}$  as a function of  $n$  for various values of  $G$  as indicated on each group of curves. Eq. (4) is represented by the thin dotted red line, Eq. (6) by the thin solid black line, and Eq. (17) by the thin solid green line; The exact results appear as thick black lines. Compare with Fig. 2 of Ref. [3].

**Table Caption**

Table I. Values of  $B_{threshold}$  for the first 4 values of mode number  $n$ ,  $n=1-4$ , as calculated from Eq. (13), Eq. (14), and exact results from Ref. [4].

$n$	Eq. (13)	Eq. (14)	Ref. [4]
1	$(45)^{1/3} \approx 3.5569$	$(80)^{1/3} \approx 4.3089$	4.4472
2	6.1297	$(252)^{1/3} \approx 6.3164$	6.5393
3	8.2354	$(576)^{1/3} \approx 8.3203$	8.5985

4	10.274	$(1100)^{1/3} \approx 10.323$	10.647
---	--------	-------------------------------	--------

Table I

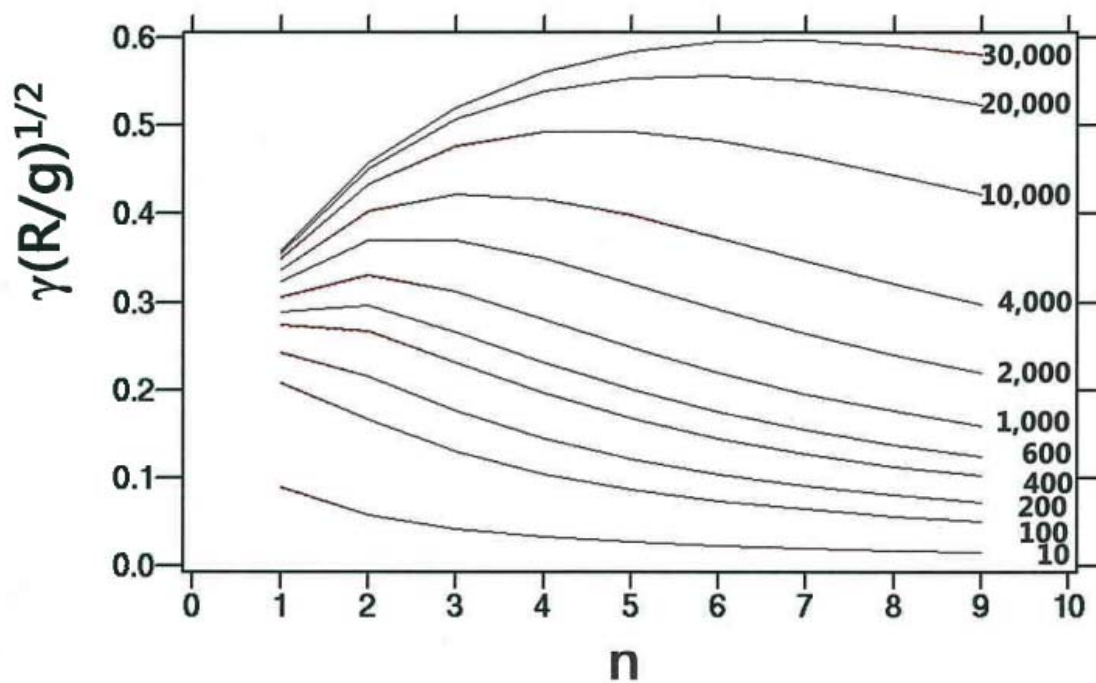


Fig. 1

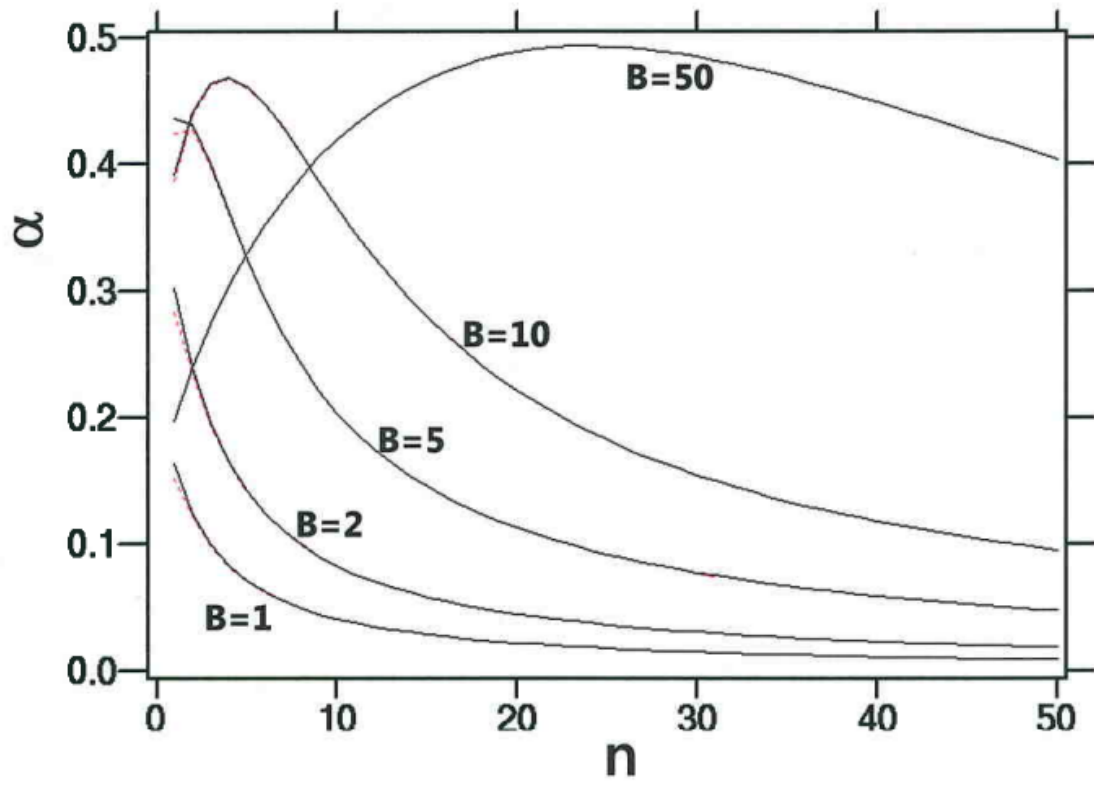


Fig. 2

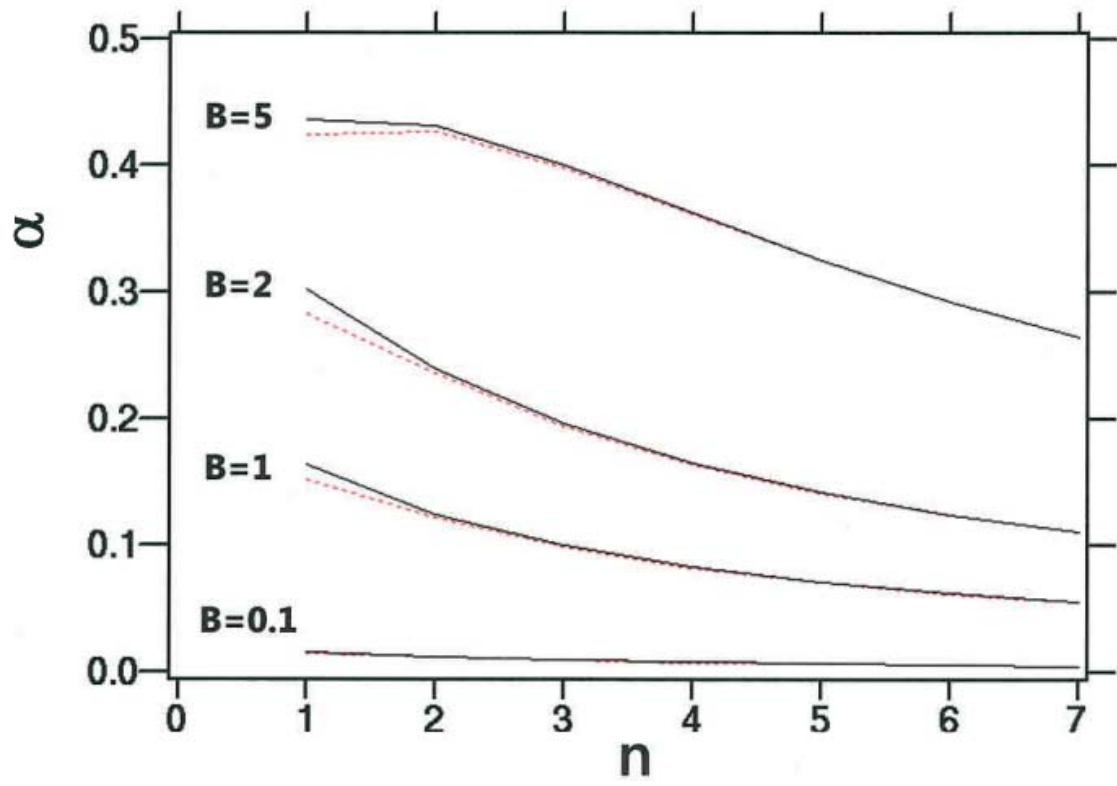


Fig. 3

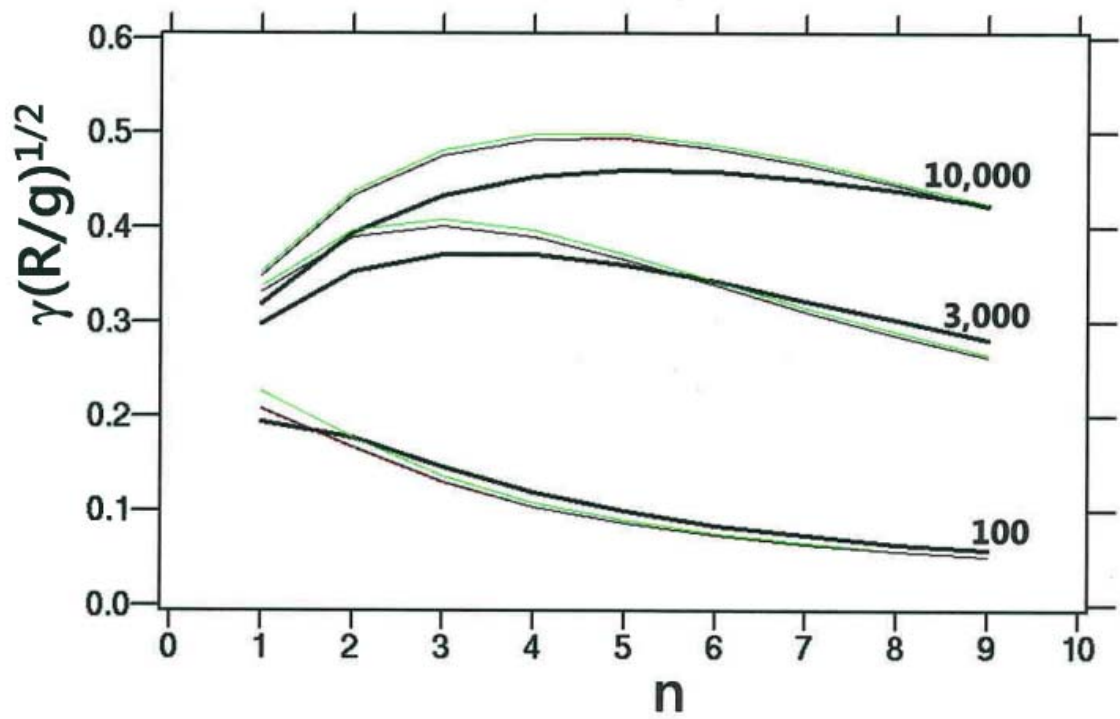


Fig. 4